Available online at www.sciencedirect.com

ScienceDirect

IFAC PapersOnline CONFERENCE PAPER ARCHIVE

IFAC PapersOnLine 52-14 (2019) 159–164

An energy-attributed graph approach for the purposes of FDI in a heated two-tank system

Kenneth R. Uren * **George van Schoor** ** **Lidia Auret** ***

* *School of Electrical, Electronic and Computer Engineering, North-West University, Potchefstroom, 2531, South-Africa. (e-mail: kenny.uren@nwu.ac.za)*

** *Unit for Energy and Technology Systems, North-West University, Potchefstroom, 2531, South-Africa. (e-mail: george.vanschoor@nwu.ac.za)*

*** *Department of Process Engineering, Stellenbosch University, Private Bag X1, Matieland, 7602, Stellenbosch, South Africa. (e-mail: lauret@sun.ac.za)*

Abstract: The focus of this paper is the development of attributed graph representations of industrial processes. In this case energy attributes are used since it serves a data reduction purpose and allows for the consideration of multi-domain systems. Pattern recognition approaches towards FDI are considered advantageous due to their visual interpretation qualities. It is therefore envisaged that these attributed graphs can be used in a new innovative graph matching methodology to be able to detect and isolate faults. A two-tank thermo-fluid system is considered in this paper as a case study. An attributed graph containing exergy and energy flows is derived and from this graph node signature matrices are extracted that represent normal and fault conditions. Fault signatures are compared to the normal signature by deriving a cost matrix using a Heterogenous Eucledian-Overlap Metric (HEOM). Eigenvalues of the cost matrices are analysed in a qualitative way as a first stage of fault detection.

Keywords: attributed graphs, energy-based, exergy flow, energy flow, fault detection

1. INTRODUCTION

Considering the current literature in the field of process monitoring it is becoming more evident that modern industrial plants are going to increasingly rely on fault monitoring and fault tolerant control schemes to produce higher quality products at higher production rates. Also, these plants need to satisfy increasingly strict safety and environmental regulations, further underpinning the requirement for advanced process monitoring schemes. Severson et al. (2015); Reis and Gins (2017) state that for future monitoring systems to be successful, they will be required to meet stringent robustness criteria, be able to cope with uncertainties and have the ability to interpret large amounts of data. Accordingly, successful approaches will likely be hybrid techniques that draw on the strengths of various methods. Another aspect that needs to be considered is the incorporation of plant operators and engineers with a monitoring scheme. It may not always be ideal to automate the entire monitoring scheme. From the literature it is evident that graphical visualisation methods can aid in communicating plant health to operators and engineers for quick fault detection and diagnosis (Gajjar and Palazoglu (2016); Du Rand et al. (2009)).

Typically the goal of any process monitoring scheme is to ensure the continuation of planned operations of a plant by providing information recognising and indicating anomalies of the plant behaviour. It is necessary to first define different types of anomalies and in this paper definitions from Isermann and Ballé (1997) will be adopted. Three types of anomalies can be distinguished: a disturbance, a fault and a failure. A disturbance can be described as an unknown and uncontrolled input acting on the system, while a fault is an un-permitted deviation of at least one characteristic property or parameter of the system from the acceptable operating conditions. A failure is a permanent interruption of the system's ability to perform a required function under specified operating conditions. Traditional control systems can normally handle disturbances within specified limits, but are not designed to cope with faults and failures. Modern fault-tolerant controllers however are being designed to account for certain classes of faults.

Normally process monitoring systems are implemented as depicted in Fig. 1. The phases in the system are to progressively determine:

(1) Fault detection - whether a fault occurred,
(2) Fault identification - which subsystems are affected,
(3) Fault diagnosis - the kind, size, location, and time of the fault, and
(4) System recovery - how to reverse the effects of the fault.

2405-8963
Peer review under responsibility of International Federation of Automatic Control.
10.1016/j.ifacol.2019.09.181

According to Russell et al. (2000) and Venkatasubramanian et al. (2003) a typical monitoring scheme contains transformations of measurements which can be based on statistical theory, pattern classification theory, information theory, and/or systems theory. Monitoring schemes can further be classified as data-driven, analytical and knowledge-based. In this sense, it is important to identify the various transformations that process measurements go through before the final diagnostic decision can be made. Two important components in the transformations are the a priori process knowledge and the search techniques used.

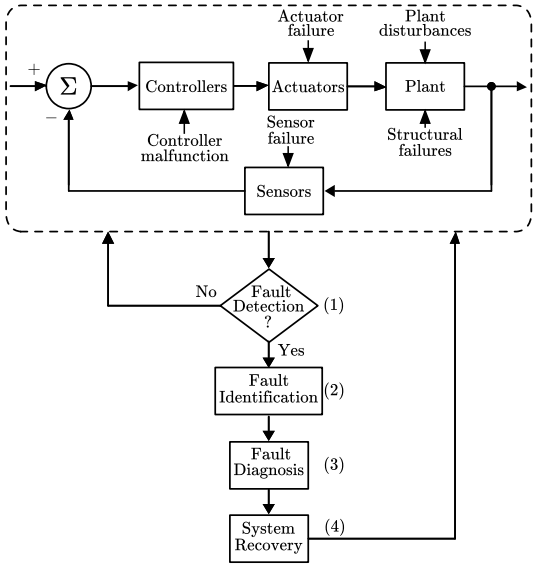

Fig. 1. High-level presentation of a process monitoring system, adopted from Russell et al. (2000); Venkatasubramanian et al. (2003)

In this paper a pattern recognition approach combined with expert knowledge in terms of energy information will be used to develop a diagnostic system. Graphs have a number of advantages when it comes to presenting system information in a structural way. Attributes deemed important from an expert point of view can be incorporated as attributes linked to nodes and links. Graph-matching may then be used as a search/optimisation technique to determine if a system is healthy by comparing healthy graphs with unhealthy or faulty graphs. Fig. 2 presents this diagnostic system. This approach fundamentally differs from the well-known bond-graph approach towards FDI Borutzky (2016); Linkens and Wang (1996). In this case a linear graph is used for structural information and system attributes. It is not used for energy-based, dynamic system modelling. The attributes assigned to the linear graph in this paper may however be energy or exergy characteristics obtained from inference measurement in an actual plant or by means of a simulation as is the case in this study.

The measurement space comprises practical measurements such as pressures, mass-flows and temperatures. No a priori problem knowledge is relating these measurements. In the feature space these measurements are functionally related by utilising a priori problem knowledge. In this paper, exergy and energy flow are considered to transform measurements to an energy feature space. Features are extracted into what is called node signature matrices

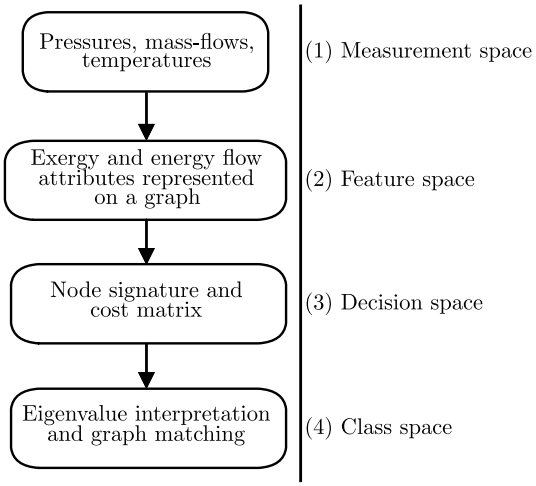

Fig. 2. Transformations part of the energy-based graph matching diagnostic approach

and then compared by means of some metric resulting in a cost matrix. The eigenvalues of the cost matrix are extracted in order to determine the character of the compared signatures. This characterisation can be interpreted in a qualitative way to detect faults. Finally a pattern recognition technique called graph matching can be used to compare measured signatures to healthy and faulty signatures in order to classify the type of fault.

This paper is organised as follows: In section 2 the process description and model used for the case study are discussed. Section 3 describes the energy attributed graph representation approach. Fault scenarios are then evaluated on the two-tank thermo-fluid system in section 4. In section 5 an overview of the envisaged energy-based graph matching methodology for FDI is considered. Finally concluding remarks are given in section 6.

2. PROCESS DESCRIPTION AND MODEL

A heated two-tank system will be considered in this paper. A diagram of the system is shown in Fig. 3(a). The outlet flow from both tanks is proportional to the square root of the level in each tank. The outlet from the first tank flows into the second tank. Each tank has its own supply of cold water with a control valve to control the level of each tank. Each tank also exchanges heat with a hot water line. The temperature in the tanks is controlled using the control valves on the hot water lines.

The main variables of interest are the flow rate of the inlet streams to the tanks, F_1 and F_2, the flow rates of the hot water in the heating coils in both tanks, F_3 and F_4, the levels of both tanks, L_1 and L_2, and the temperatures of both tanks, T_1 and T_2. F_1 and F_2 are used as manipulated variables (MVs) to control L_1 and L_2 respectively. F_3 and F_4 are used as MVs to control T_1 and T_2 respectively. The controllers used are simple proportional integral derivative (PID) controllers that change the values of the MVs according to the deviation of the controlled variables (CVs) from their set-points (SPs). The mass balance of the first tank is given by

$$\frac{dV_1}{dt} = F_1 - F_{1,\text{out}}, \tag{1}$$

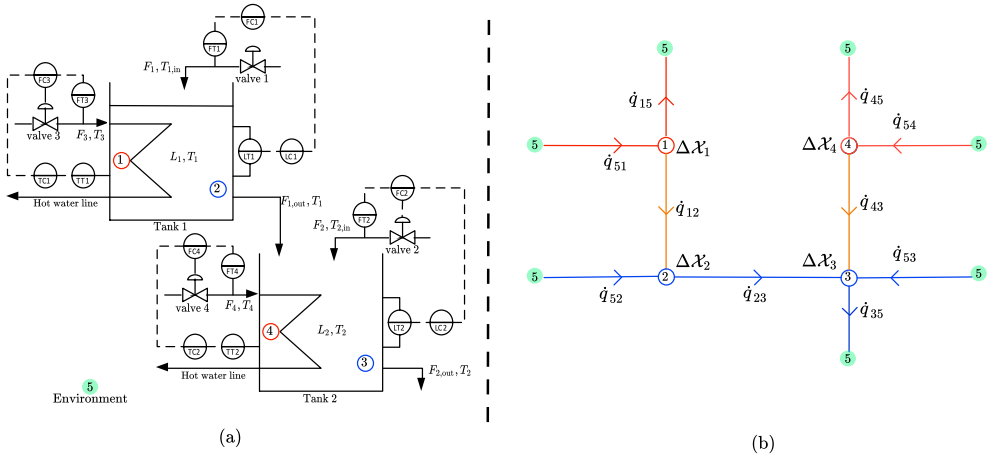

Fig. 3. (a) Two-tank thermo-fluid system (b) Energy-based attributed graph

with V_1 the volume of tank 1, given by the level multiplied by the cross sectional area. The level varies, so it remains within the derivative term, but the area can be removed. The flow rate of tank 1 is dependent on the level of the tank (L_1). The flow rate is related to the pressure driving force (Marlin (2000)), i.e. the static pressure exerted by the liquid. This relationship can be approximated by

$$F_{1,\text{out}} = k_L \cdot \sqrt{L_1}. \tag{2}$$

Substituting (2) into (1) results in the mass balance for tank 1, given by

$$A_1 \frac{dL_1}{dt} = F_1 - k_L \cdot \sqrt{L_1}, \tag{3}$$

with A_1 the cross-sectional area of tank 1. For the second tank the mass balance is similar, except that the underflow from tank 1 also flows into the second tank. The resulting mass balance for tank 2 is given by

$$A_2 \frac{dL_2}{dt} = k_L \cdot \sqrt{L_1} + F_2 - k_L \cdot \sqrt{L_2}, \tag{4}$$

with A_2 the cross-sectional area of tank 2. The energy balance of the system can be written in general form as follows:

$$\frac{dU}{dt} = \dot{H}_{\text{in}} - \dot{H}_{\text{out}} + Q. \tag{5}$$

The change in internal energy, U, with time is given by

$$\frac{dU}{dt} = \rho C_p \frac{dVT}{dt}. \tag{6}$$

The enthalpy of for example stream i, is given by

$$H_i = \rho C_p F_i (T_i - T_{\text{ref}}). \tag{7}$$

Substituting these equations into the energy balance, assuming a value of 0 for T_{ref}, results in the following equation for the first tank:

$$\rho C_p \frac{dV_1 T_1}{dt} = \rho C_p \left(F_1 \cdot T_{1,\text{in}} - F_{1,\text{out}} \cdot T_1\right) + Q. \tag{8}$$

Under the assumption of perfect mixing in the tank the temperature of the stream flowing out of the tank is equal to the temperature in the tank. Q represents the heat transferred to the liquid in the tank from the liquid in the heating coils. An energy balance on the liquid in the heating coils is given by

$$Q = \rho C_p F_3 (T_3 - T_{\text{out}}), \tag{9}$$

with ρ and C_p, the density and heat capacity respectively. F_3 is the flow rate of the hot water stream line, T_3 is the temperature at which the stream enters the coils and T_{out} is the temperature at which the fluid exits the tank on the heating coil side. Rearranging (9) so that T_{out} is the subject of the equation results in

$$T_{\text{out}} = T_3 - \frac{Q}{\rho C_p F_3}. \tag{10}$$

The heat transferred can be determined using the overall heat transfer coefficient, UA. Assuming that the inner film resistance dominates the heat transfer through the coils, and that the resistance of the tube walls and the outer film resistance are negligible, an empirical equation relating the heat transfer coefficient to the flow rate of a liquid can be determined as follows (Marlin, 2000):

$$UA = aHeat \cdot F_3^b. \tag{11}$$

The heat transfer from the pipes is then given by the heat transfer coefficient multiplied by an approximation of the mean difference of the temperature in the tank and the temperature in the coils resulting in

$$Q = -aHeat \cdot F_3^b \left(\frac{(T_1 - T_3) + (T_1 - T_{\text{out}})}{2} \right). \tag{12}$$

$aHeat$ and b are constants for heat transfer calculation and are specified according to Table 1. Combining (10) and (12) to eliminate T_{out} results in

$$Q = -\frac{aHeat \cdot F_3^{b+1}}{F_3 + \frac{aHeat \cdot F_3^b}{2\rho C_p}} \cdot (T_1 - T_3). \tag{13}$$

Table 1. Parameters used in model of two-tank system

Parameter	Description	Value	Units
$aHeat$	Constant for heat transfer coefficient calculation	1.41×10^5	[cal/(min °C)]
b	Constant for heat transfer coefficient calculation	0.5	[-]
C_p	Heat capacity of water	1	[cal/(g °C)]
ρ	Density of water	10^6	[g/m^3]
A_1	Cross-sectional area of tank 1	1	[m^2]
A_2	Cross-sectional area of tank 2	1	[m^2]
k_L	Level constant	0.128	[m^3/min/m$^{0.5}$]

Substituting (13) into (8) results in the complete energy balance of tank 1 as given by

$$\rho C_p \frac{dV_1 T_1}{dt} = \rho C_p \left(F_1 \cdot T_{1,\text{in}} - F_{1,\text{out}} \cdot T_1\right) - \frac{aHeat \cdot F_3^{b+1}}{F_3 + \frac{aHeat \cdot F_3^b}{2\rho C_p}} \cdot (T_1 - T_3). \quad (14)$$

For tank 2 the energy balance is similar, except that the energy entering the system from the outlet stream of tank 1 has to be included. The flow rate of water into the tank is F_2, entering at a temperature of $T_{2,\text{in}}$. The flow rate of the hot water is F_4, entering at a temperature of T_4. The temperature of the tank is T_2. The energy balance of tank 2 is therefore given by

$$\rho C_p \frac{dV_2 T_2}{dt} = \rho C_p \left(F_{1,\text{out}} \cdot T_1 + F_2 \cdot T_{2,\text{in}} - F_{2,\text{out}} \cdot T_2\right) - \frac{aHeat \cdot F_4^{b+1}}{F_4 + \frac{aHeat \cdot F_4^b}{2\rho C_p}} \cdot (T_2 - T_4). \quad (15)$$

The steady state values for variables in the process are given in Table 2. The steady state values for the CVs, L_1, L_2, T_1 and T_2, are also their set-point values.

Table 2. Steady state values for the two-tank system model

Variable	Value	Units
L_1	2.00	[m]
L_2	3.00	[m]
T_1	50.00	[°C]
T_2	50.00	[°C]
$T_{1,\text{in}}$	25.00	[°C]
$T_{2,\text{in}}$	25.00	[°C]
T_3	100.00	[°C]
T_4	100.00	[°C]
F_1	0.181	[m^3/min]
F_2	0.0408	[m^3/min]
F_3	0.5	[m^3/min]
F_4	0.04	[m^3/min]
$F_{1,\text{out}}$	0.191	[m^3/min]
$F_{2,\text{out}}$	0.222	[m^3/min]

The values of the parameters used in the model are given in Table 1. The value for the proportionality constant relating the underflow to the level, k_L, was determined by substituting steady-state values into (3) and solving for k_L (at steady state the differential term is 0). The valve constant for each control valve was simply chosen so that the steady state value of the flow rate being controlled by the valve corresponded to a valve position of 50 %.

This model is implemented in the Matlab® and Simulink® environment to be used for evaluating the fault detection and diagnosis scheme discussed in the following section. In this paper sensor noise is not considered in the simulation model. The complete simulation code can be found on the github repository, see Lindner and Auret (2017) and a discussion of the model is given in Lindner et al. (2017).

3. ENERGY ATTRIBUTED GRAPH REPRESENTATION APPROACH

Let an attributed graph be defined as $G_{\mathcal{A}} = (\mathcal{N}, \mathcal{L}, \mathcal{A})$, where $\mathcal{N}$ is a finite non-empty set of nodes (also called vertices), $\mathcal{L}$ is a finite set of links (also called edges) and $\mathcal{A}$ the attribute set. Let $n_i \in \mathcal{N}$ be called a node and i the node number, and $l_j \in \mathcal{L}$ be called a link and j the link number. Then, the attribute set is defined as $\mathcal{A} = \{a_{n_i}, a_{l_{ij}}\}$ where

- a_{n_i} is the attribute of the node n_i,
- $a_{l_{ij}}$ are the set of link attributes incident to n_i. Each link is assigned a direction by means of arrows:
  - If the link direction is away from the node, the link attribute is multiplied by $+1$.
  - If the link direction is towards the node, the link attribute is multiplied by -1.

An energy-attributed graph for the two-tank system is depicted in Fig. 3(b). The change in exergy flow rate, $\Delta\mathcal{X}$, and the energy flow rate, $\dot{q}$, are considered as the node and link attributes respectively. From Fig. 3(b) five nodes of interest are identified namely:

(1) The hot water pipe transferring heat to tank 1
(2) Tank 1
(3) The hot water pipe transferring heat to tank 2
(4) Tank 2
(5) The environment node

The energy flows are indicated by links and numbered according to the related incident nodes. Let the energy flow rate from node p to node q be defined as

$$\dot{q}_{pq} = \dot{m}_{pq}(h_p - h_q). \quad (16)$$

The mass flow rate and enthalpy are indicated as $\dot{m}$ and h respectively. The energy flow rates (with unit [J/s] or [W]) between the hot water pipe and the tanks may be specifically defined as

$$\dot{q}_{12} = \frac{aHeat F_3^{b+1}}{F_3 + \frac{aHeat F_3^b}{2\rho C_p}} \cdot (T_1 - T_3), \quad (17)$$

$$\dot{q}_{43} = \frac{aHeat F_4^{b+1}}{F_4 + \frac{aHeat F_4^b}{2\rho C_p}} \cdot (T_2 - T_4). \quad (18)$$

Also, exergy flow rate (with unit [J/s] or [W]) is defined as

$$\mathcal{X} = \dot{m}[(h - h_0) - T_0(s - s_0)], \quad (19)$$

where entropy is indicated as s and the subscript 0 references variables at environmental conditions. Equation (20) defines the change in exergy flow rate as the exergy flow rate at the node exit minus the exergy flow rate at the node inlet.

$$\Delta\mathcal{X} = \mathcal{X}_{\text{out}} - \mathcal{X}_{\text{in}} \quad (20)$$

Next a general node signature matrix, $\mathbf{N_s}$ for the attributed graph in Fig. 3(b) can be derived as

$$\mathbf{N_s} = \left[\begin{array}{c|ccccc} \Delta\mathcal{X}_1 & \dot{q}_{11} & \dot{q}_{12} & \dot{q}_{13} & \dot{q}_{14} & \dot{q}_{15} \\ \Delta\mathcal{X}_2 & \dot{q}_{21} & \dot{q}_{22} & \dot{q}_{23} & \dot{q}_{24} & \dot{q}_{25} \\ \Delta\mathcal{X}_3 & \dot{q}_{31} & \dot{q}_{32} & \dot{q}_{33} & \dot{q}_{34} & \dot{q}_{35} \\ \Delta\mathcal{X}_4 & \dot{q}_{41} & \dot{q}_{42} & \dot{q}_{43} & \dot{q}_{44} & \dot{q}_{45} \\ \Delta\mathcal{X}_5 & \dot{q}_{51} & \dot{q}_{52} & \dot{q}_{53} & \dot{q}_{54} & \dot{q}_{55} \end{array}\right]. \quad (21)$$

For this specific case the node signature matrix is presented as

$$\mathbf{N_s} = \left[\begin{array}{c|ccccc} \Delta\mathcal{X}_1 & 0 & \dot{q}_{12} & 0 & 0 & \dot{q}_{15} \\ \Delta\mathcal{X}_2 & \dot{q}_{21} & 0 & \dot{q}_{23} & 0 & \dot{q}_{25} \\ \Delta\mathcal{X}_3 & 0 & \dot{q}_{32} & 0 & \dot{q}_{34} & \dot{q}_{35} \\ \Delta\mathcal{X}_4 & 0 & 0 & \dot{q}_{43} & 0 & \dot{q}_{45} \\ 0 & \dot{q}_{51} & \dot{q}_{52} & \dot{q}_{53} & \dot{q}_{54} & 0 \end{array}\right]. \quad (22)$$

Considering the convention as described, the node signature matrix can be rewritten as

$$\mathbf{N}_s = \left[\begin{array}{c|ccccc} \Delta\mathcal{X}_1 & 0 & \dot{q}_{12} & 0 & 0 & \dot{q}_{15} \\ \Delta\mathcal{X}_2 & -\dot{q}_{12} & 0 & \dot{q}_{23} & 0 & -\dot{q}_{52} \\ \Delta\mathcal{X}_3 & 0 & -\dot{q}_{23} & 0 & -\dot{q}_{43} & \dot{q}_{35} \\ \Delta\mathcal{X}_4 & 0 & 0 & \dot{q}_{43} & 0 & \dot{q}_{45} \\ 0 & \dot{q}_{51} & \dot{q}_{52} & \dot{q}_{53} & \dot{q}_{54} & 0 \end{array}\right]. \quad (23)$$

As can be seen from (22) the node signature matrix partitions the node and link attributes. Links not connected or used are made zero. The change in exergy flow rate of the environment node is assumed zero.

For graph matching purposes a node signature matrix is generated for both normal and fault conditions. These matrices are indicated by $\mathbf{N}_{s,n}$ and $\mathbf{N}_{s,f}$ respectively. In order to compare these signature matrices a distance metric needs to be defined. Although several distance metrics are proposed by Wilson and Martinez (1997); Jouili et al. (2009), the most commonly used metrics are suitable only for either symbolic or numeric attributes. These include the Euclidean and Manhattan distance metrics for numeric attributes, and the Overlap distance for symbolic attributes. In order to keep the metric as general as possible a metric is chosen that will be able to handle both symbolic and numerical attributes. Such a metric is generally known as a heterogeneous distance function. One particular metric that has this property is called the Heterogeneous Euclidean-Overlap Metric (HEOM).

The comparison of two graphs is therefore achieved by comparing each row vector in the normal node signature matrix with the corresponding row vector in the faulty node signature matrix. The HEOM metric for this comparison is given by

$$HEOM(\mathbf{N}_{s,n}, \mathbf{N}_{s,f}) = \sqrt{\sum_{a=1}^{k} \delta(\mathbf{N}_{s,n}(i,a), \mathbf{N}_{s,f}(j,a))^2}, \quad (24)$$

where $\mathbf{N}_{s,n}(i,a)$ refers to the (i,a) entry in the normal signature matrix, and $\mathbf{N}_{s,f}(j,a)$ refers to the (j,a) entry in the faulty signature matrix. a refers to the a-th column entry of the rows considered, k is the length of the row and the function δ for a numeric attributes only case is given by

$$\delta(\mathbf{N}_{s,n}(i,a), \mathbf{N}_{s,f}(j,a)) = \frac{|\mathbf{N}_{s,n}(i,a) - \mathbf{N}_{s,f}(j,a)|}{range_a}, \quad (25)$$

where $range_a$ is used to normalise the attributes, and is defined as

$$range_a = max_a - min_a, \quad (26)$$

where max_a and min_a are the maximum and minimum values respectively observed in the a-th column entry.

All metric evaluations are then gathered in a cost matrix, $\mathbf{C}$, defined as

$$\mathbf{C}(\mathbf{N}_{s,n}, \mathbf{N}_{s,f}) = [HEOM(\mathbf{N}_{s,n}, \mathbf{N}_{s,f})], \quad (27)$$

which is a square matrix with dimension equal to the number of nodes. Let $\mathbf{C}(\mathbf{N}_{s,n}, \mathbf{N}_{s,f1})$ be the cost matrix related to a fault number 1. Then, the eigenvalues of this cost matrix can be calculated and represented by λ_{f1}. If k faults are considered, then a matrix containing the k sets of eigenvalues can be derived as follows

$$\mathbf{\Lambda}_F = [\lambda_n, \lambda_{f1}, \ldots, \lambda_{fk}], \quad (28)$$

where λ_n represents the eigenvalues of the normal cost matrix. Λ_F will be called the fault eigenvalue matrix. Each row fo the eigenvalue matrix is then normalised with respect to the corresponding eigenvalue of λ_n. This will allow both ease of interpretation and fair comparison.

Then comparing the fault eigenvalues to that of the normal eigenvalues in a qualitative way, a qualitative fault signature matrix $\mathbf{Q}_F$ can be derived. Each entry of $\mathbf{Q}_F$ can be determined as follows:

$$\mathbf{Q}_F(i,j) = \begin{cases} + \text{ if the eigenvalue of } \lambda_f > \lambda_n \\ - \text{ if the eigenvalue of } \lambda_f < \lambda_n \\ 0 \text{ if the eigenvalue of } \lambda_f = \lambda_n \end{cases} \quad (29)$$

A fault is then detectable if at least one set of fault eigenvalues is different from the normal set of eigenvalues, and a fault is isolable if its set of fault eigenvalues is different from all the others.

4. CASE STUDY OF FAULT SCENARIOS

The monitoring objectives are to detect and possibly isolate 5 faults listed as follows:

(a) Two sensor faults affecting the tank level sensor, and the temperature sensor.
(b) Two actuator faults. The first fault is related to the heat transfer from the hot water side to the tank, generally called fouling. The second fault is valve failure.
(c) A process fault in the form of tank leakage.

These faults will first be induced one at a time for tank 1 and then for tank 2.

For each fault induced the corresponding cost matrix is calculated. The eigenvalues of each fault cost matrix is then extracted. These eigenvalues are grouped in the normalised fault eigenvalue matrix. Let the normal and fault conditions be represented as follows:

(1) $\mathcal{N}$ = Normal state, no faults case.
(2) $\mathcal{F}_1$ = Tank level sensor fault (5 % bias error).
(3) $\mathcal{F}_2$ = Tank temperature sensor fault (5 % bias error).
(4) $\mathcal{F}_3$ = 5 % change in the heat transfer coefficient $aHeat$ in order to simulate fouling.
(5) $\mathcal{F}_4$ = Valve failure; valve got stuck on its original steady-state value. The valve controlling the cold liquid flow into the tank is considered.
(6) $\mathcal{F}_5$ = Tank leakage.

4.1 Tank1

After inducing these faults in tank 1, the following normalised fault eigenvalue matrix is obtained:

$$\mathbf{\Lambda}_F = \left[\begin{array}{c|c|c|c|c|c} \mathcal{N} & \mathcal{F}_1 & \mathcal{F}_2 & \mathcal{F}_3 & \mathcal{F}_4 & \mathcal{F}_5 \\ 1.0000 & 0.9644 & 0.9667 & 0.9382 & 1.2035 & 1.4739 \\ 1.0000 & 0.9559 & 0.9573 & 0.9278 & 1.2382 & 1.5469 \\ 1.0000 & 1.0474 & 1.0506 & 1.0243 & 0.8572 & 1.0085 \\ 1.0000 & 0.9192 & 0.9676 & 0.9814 & 1.4609 & 0.1628 \\ 1.0000 & 0.8905 & 0.9300 & 0.9672 & 1.1610 & -0.0357 \end{array}\right]. \quad (30)$$

By comparing the fault eigenvalues to the normal eigenvalues in a qualitative way, a qualitative fault signature matrix is obtained:

$$\mathbf{Q}_F = \left[\begin{array}{c|c|c|c|c} \mathcal{F}_1 & \mathcal{F}_2 & \mathcal{F}_3 & \mathcal{F}_4 & \mathcal{F}_5 \\ \hline - & - & - & + & + \\ - & - & - & + & + \\ + & + & + & - & + \\ - & - & - & + & - \\ - & - & - & + & - \end{array}\right]. \tag{31}$$

From (31) it can firstly be seen that all faults are detectable. Faults $\mathcal{F}_1$, $\mathcal{F}_2$, and $\mathcal{F}_3$ are not isolable from each other, but $\mathcal{F}_4$ and $\mathcal{F}_5$ are isolable.

4.2 Tank 2

After inducing these faults in tank 2 the following normalised fault eigenvalue matrix is obtained:

$$\mathbf{\Lambda}_F = \left[\begin{array}{c|c|c|c|c|c} \mathcal{N} & \mathcal{F}_1 & \mathcal{F}_2 & \mathcal{F}_3 & \mathcal{F}_4 & \mathcal{F}_5 \\ \hline 1.0000 & 0.9897 & 0.9849 & 0.9940 & 0.9440 & 0.9961 \\ 1.0000 & 0.9923 & 0.9904 & 0.9955 & 0.9583 & 0.9953 \\ 1.0000 & 0.9615 & 0.9317 & 0.9774 & 0.7796 & 1.0025 \\ 1.0000 & 1.0255 & 1.0141 & 1.0149 & 1.2014 & 0.9998 \\ 1.0000 & 1.0091 & 1.0139 & 1.0073 & 1.1164 & 0.9998 \end{array}\right] \tag{32}$$

For the case shown in (32) the resulting qualitative fault signature matrix is given by

$$\mathbf{Q}_F = \left[\begin{array}{c|c|c|c|c} \mathcal{F}_1 & \mathcal{F}_2 & \mathcal{F}_3 & \mathcal{F}_4 & \mathcal{F}_5 \\ \hline - & - & - & - & - \\ - & - & - & - & - \\ - & - & - & - & + \\ + & + & + & + & - \\ + & + & + & + & - \end{array}\right]. \tag{33}$$

Again all faults are detectable, however, in this case faults $\mathcal{F}_1$ up to $\mathcal{F}_4$ are not isolable. Only $\mathcal{F}_5$ is isolable.

5. CONCLUSION

In this paper an attributed graph, containing exergy and energy flow rates, was considered. Node signature matrices were extracted from this graph for normal and faulty cases. A cost matrix was then obtained by using an HEOM norm. This cost matrix will serve as the input for the energy-based graph matching methodology, but for this paper the cost matrix was analysed following an eigenvalue extraction and qualitative interpretation approach. It was shown that fault detection was possible, but the isolability of the faults could still be improved. Since the isolabiltiy was more challenging for the second tank, further investigation is needed to determine why this is the case. It is proposed that thresholds should be added to increase isolability. Another interesting option is combining this graph-based approach with statistical techniques such as PCA. It has been shown that this hybrid approach has improved fault isolation properties as indicated in the paper by Smaili et al. (2014). Also, a sensitivity analysis and a comparison to other existing FDI techniques are required to evaluate the proposed technique.

ACKNOWLEDGEMENTS

This work is based on the research supported by Sasol Limited, South Africa. We would also like to acknowledge the Department of Process Engineering at Stellenbosch University for the use of the Simulink® model simulation.

REFERENCES

Borutzky, W. (2016). *Bond Graphs for Modelling, Control and Fault Diagnosis of Engineering Systems*. Springer International Publishing.

Du Rand, C.P., van Schoor, G., and Nieuwoudt, C. (2009). Enthalpy-entropy graph approach for the classification of faults in the main power system of a closed Brayton cycle HTGR. *Annals of Nuclear Energy*, 36(6), 703–711.

Gajjar, S. and Palazoglu, A. (2016). A data-driven multidimensional visualization technique for process fault detection and diagnosis. *Chemometrics and Intelligent Laboratory Systems*, 154, 122–136.

Isermann, R. and Ballé, P. (1997). Trends in the application of model based fault detection and diagnosis of technical processes. *Control Eng. Practice*, 5(5), 709–719. doi:10.1016/S0967-0661(97)00053-1.

Jouili, S., Mili, I., and Tabbone, S. (2009). Attributed graph matching using local descriptions. In *ACIVS*, volume 5807, 89–99. Springer.

Lindner, B., Auret, L., and Bauer, M. (2017). Investigating the impact of perturbations in chemical processes on data-based causality analysis. part 2: Testing granger causality and transfer entropy. *IFAC-PapersOnLine*, 50(1), 3275–3280.

Lindner, B. and Auret, L. (2017). IFAC causality analysis. `https://github.com/ProcessMonitoringStellenboschUniversity/IFAC-Causality-Analysis`.

Linkens, D. and Wang, H. (1996). *Intelligent Supervisory Control, A Qualitative Bond Graph Reasoning Approach*. World Scientific Series In Robotics And Intelligent Systems. World Scientific Publishing Company.

Marlin, T. (2000). *Process control: designing processes and control systems for dynamic performance*. McGraw-Hill chemical engineering series. McGraw-Hill.

Reis, M.S. and Gins, G. (2017). Industrial process monitoring in the big data/industry 4.0 era: from detection, to diagnosis, to prognosis. *Processes*, 5(3), 35.

Russell, E.L., Chiang, L.H., and Braatz, R.D. (2000). *Fault detection and diagnosis in industrial systems*. Springer Science & Business Media.

Severson, K., Chaiwatanodom, P., and Braatz, R.D. (2015). Perspectives on process monitoring of industrial systems. *IFAC-PapersOnLine*, 28(21), 931–939. doi:10.1016/j.ifacol.2015.09.646.

Smaili, R., Harabi, R.E., and Abdelkrim, M. (2014). Fault diagnosis based on graphical tools for multi-energy processes. *IFAC Proceedings Volumes*, 47(3), 7073 – 7078. 19th IFAC World Congress.

Venkatasubramanian, V., Rengaswamy, R., Yin, K., and Kavuri, S.N. (2003). A review of process fault detection and diagnosis. *Computers & Chemical Engineering*, 27(3), 293–311. doi:10.1016/S0098-1354(02)00160-6.

Wilson, D.R. and Martinez, T.R. (1997). Improved heterogeneous distance functions. *Journal of artificial intelligence research*.